

Observation of optical absorption correlated with surface state of topological insulator

Jiwon Jeon,¹ Kwangnam Yu,¹ Jiho Kim,¹ Jisoo Moon,² Seongshik Oh,² and E. J. Choi^{1,*}

¹*Department of Physics, University of Seoul, Seoul 130-743, Korea*

²*Department of Physics and Astronomy, Rutgers,
the State University of New Jersey, Piscataway, New Jersey 08854, USA*

(Dated: June 6, 2022)

We performed broadband optical transmission measurements of Bi_2Se_3 and In-doped $(\text{Bi}_{1-x}\text{In}_x)_2\text{Se}_3$ thin films, where in the latter the spin-orbit coupling (SOC) strength can be tuned by introducing In. Drude and interband transitions exhibit In-dependent changes that are consistent with evolution from metallic ($x=0$) to insulating ($x=1$) nature of the end compounds. Most notably, an optical absorption peak located at $\hbar\omega=1\text{eV}$ in Bi_2Se_3 is completely quenched at $x=0.06$, the critical concentration where the phase transition from TI into non-TI takes place. For this x , the surface state (SS) is vanished from the band structure as well. The correlation between the 1eV optical peak and the SS in the x -dependences suggests that the peak is associated with the SS. We further show that when Bi_2Se_3 is electrically gated, the 1eV-peak becomes stronger(weaker) when electron is depleted from (accumulated into) the SS. These observations combined together demonstrate that under the $\hbar\omega=1\text{eV}$ illumination electron is excited from a bulk band into the topological surface band of Bi_2Se_3 . The optical population of surface band is of significant importance not only for fundamental study but also for TI-based optoelectronic device application.

Introduction. Topological insulator (TI) is a novel state of matter characterized by insulating bulk and metallic surface[1–5]. The surface state, topologically protected and chirally-textured, supports dissipationless spin-conserving current, applicable for quantum devices[6–8]. Optically, various kinds of electron transitions occur in a TI under photo illumination both in the surface and in the bulk as demonstrated by numerous previous experiments: For the archetypal TI material Bi_2Se_3 , intraband (Drude) transition and Kerr rotation of the surface carrier were observed in THz measurement [9]. In the infrared range, Post *et al* measured the interband transition from bulk valence-band (VB) to bulk conduction-band (CB), VB→CB, and determined upper bound of Drude weight of SS [10]. Also Falsetti *et al* observed the infrared Berreman resonance of the surface electron in Bi_2Se_3 thin films [11]. On the other hand, for periodically modulated Bi_2Se_3 , plasmonic excitation of the surface electron [12] and the plasmon-phonon interaction [13] were observed at THz frequencies.

One interesting optical absorption that TI can host yet has not been detected is an excitation of electron from bulk band into SS. This particular transition between bulk and surface, VB→SS, will provide rare opportunity to study how the surface and bulk are connected optically. Also, when the surface electron is populated by this optical transition, the surface electron is increased and therefore the topological current (\propto surface electron) is enhanced, which can boost the performance of TI as optoelectronic device such as photogalvanics and optical imaging display [14, 15]. In fact Sobota *et al* showed that a similar transition can occur from bulk CB to 2nd SS, CB→2nd SS, at a visible frequency [16]. (Here the 2nd SS

refers to another SS that lies above the 1st or fundamental SS). However the optical transition into the 1st SS or fundamental SS, VB→SS, was not reported yet. It is not clear at this point whether the lack of the SS-populating optical transition is due to that other transition such as VB→CB is overwhelmingly stronger, making the detection difficult [17], or more fundamentally, this particular transition is forbidden by optical selection rule.

Here we performed broadband optical absorption measurement of Bi_2Se_3 and $(\text{Bi}_{1-x}\text{In}_x)_2\text{Se}_3$ thin films from far-IR to UV frequencies. In $(\text{Bi}_{1-x}\text{In}_x)_2\text{Se}_3$, the spin-orbit coupling (SOC) strength is modulated by means of the indium (In) substitution. As In-content is increased the SOC of Bi_2Se_3 is decreased and consequently the topological property is softened. Eventually, at certain substitution level, the topological SS is completely quenched from the band structure. Accordingly any SS-related optical transition will be removed from the wide-range optical excitation spectrum, which in fact offers us an invaluable means to find the SS-population transition in particular. Our measurement shows signatures that such optical absorption may exist.

Experiment. High quality epitaxial Bi_2Se_3 and $(\text{Bi}_{1-x}\text{In}_x)_2\text{Se}_3$ thin films were grown on Al_2O_3 and SiO_2/Si substrates using the MBE method [18]. Optical transmittance $T(\omega)$ was measured from Far-infrared to UV by using Fourier transform infrared spectroscopy (FTIR) spectrometer in combination with spectroscopic ellipsometer. For gate-dependent optical measurement gate-voltage V_G was applied between Bi_2Se_3 and Si of the substrate. Optical conductivity $\sigma_1(\omega)$ was calculated from transmission data through rigorous Kramers-Kronig transformation by using RefFit[19]. The experimental details are described in Supplemental Material 1[20] and references therein.

* echoi@uos.ac.kr

Results. Figure 1 shows the wide-range optical conductivity $\sigma_1(\omega)$ of the 50QL-thick Bi₂Se₃ film. In the Far-infrared region, $\sigma_1(\omega)$ consists of Drude absorption and optical phonon peak, both coming from the bulk, where the former one arises from the Se-vacancy driven carrier [21, 22]. For $\hbar\omega > 0.25\text{eV}$, the interband (IB) transition VB→CB leads to the rapid rise of $\sigma_1(\omega)$. Note that there is an absorption peak at $\hbar\omega=1\text{eV}$ (\equiv Peak-A hereafter) which we will pay particular attention to.

In Figure 2 we show optical conductivity measured for a series of In-substituted (Bi_{1-x}In_x)₂Se₃ films. The In-concentration x was varied for $0 \leq x \leq 0.9$ range. Previous studies showed that as Bi is replaced by the light element In, the spin-orbit interaction is reduced and the topological property of Bi₂Se₃ becomes weaker [23–26]. At a critical concentration x_c , phase transition from TI to non-TI (NTI) phase occurs where the bulk band gap is closed, and CB and VB begin to reinvert. The x_c lies between $x=0.04$ and $x=0.06$ depending on the film thickness, and for at $x \geq x_c$ the topological SS is completely vanished [23, 24]. The $\sigma_1(\omega)$ shows that Peak-A becomes weaker as x increases. For quantitative analysis of this behavior we isolate Peak-A by removing background conductivity from $\sigma_1(\omega)$ as $\sigma_1^A(\omega) = \sigma_1(\omega) - \sigma_1^{BG}(\omega)$ as illustrated in the inset of Figure 2d, (a polynomial function was used for the σ_1^{BG}) and calculated the strength of Peak-A as $S = \int \sigma_1^A(\omega) d\omega$. Figure 2d shows that S is quenched at $x=0.06$. To double check this behavior we performed independent analysis of Peak-A: we calculate the second derivative $\frac{d^2\sigma_1}{dE^2}$ and measure the distance (w) and depth (d) of the extrema pattern, which allows determination of strength S ($= \frac{1}{12} \sqrt{\frac{\pi}{6}} \cdot dw^3$) as well as width ($= \frac{1}{\sqrt{3}} \cdot w$) and height ($= \frac{1}{12} \cdot dw^2$) of Peak-A. (See Supplemental Fig. S1 for details[20]). The S is quenched at $x=0.06$ again, which confirms the $S = \int \sigma_1^A(\omega) d\omega$ analysis. Importantly $x=0.06$ is the critical x_c for the TI→NTI transition for the thickness $d=50\text{QL}$ of our films: that is, the SS is vanished at this x . This correlation of Peak-A with the TI→NTI transition strongly suggests that Peak-A is related with the topological SS of Bi₂Se₃. We emphasize that this behavior is strikingly different from those of the other optical absorption features: In Supplemental Fig.S2[20], we show that the Drude absorption is vanished at $x \sim 0.5$, the phonon peak splits at $x=0.12$, and the IB survives up to $x=0.9$. (For $x=1$, In₂Se₃ is a large gap band insulator with $E_g > 1.5\text{eV}$) Note that none of these features are correlated with x_c . In contrast Peak-A manifests clear correlation with x_c and is the only absorption of such kind.

Given the correlation of Peak-A with SS, one can propose possible pictures on how Peak-A is created. Specifically, Peak-A can arise when (1) SS electron is excited into empty state lying 1eV above, or alternatively (2) electron lying at 1eV below is excited into the SS. In both scenarios Peak-A becomes extinct when

SS is suppressed at x_c . To find out which scenario is correct, we performed electrical gating experiment on the Bi₂Se₃ film ($d=8\text{QL}$). For this a Bi₂Se₃ film was grown on SiO₂/Si substrate and optical transmission was measured while gate voltage V_G is applied between the film and Si. In this back-gate configuration, the Fermi energy E_F shifts down (up) for the negative (positive) V_G due to electron depletion (accumulation) in the film. Fig.3(b) shows that $T(V_G)/T(0)$ changes in the Far-IR, mid-IR, and at 1eV. Figure 3(c) shows that Peak-A becomes stronger (weaker) for negative (positive) V_G . Such change supports the scenario (2) over (1) for the following reason: For $V_G < 0$ the electron occupation of SS is reduced and more empty SS become available, which strengthens the transition of (2), which agrees with the increase of Peak-A strength. This relation is visualized in Fig.4. In the scenario (1), on the other hand, the surface electron is decreased and the peak becomes weaker, opposite to the observed behavior of Peak-A. Therefore, the V_G -dependent result demonstrates that Peak-A arises most likely by excitation of electron from a state lying 1eV below into the SS. In this transition electron occupation of SS is increased, or equally, the SS is optically populated by illuminating Bi₂Se₃ with $\hbar\omega=1\text{eV}$. Here we remark that the V_G -dependent change in Figure 3c is very small, less than even 0.1%. Nevertheless the Peak-A change is successfully measured, demonstrating the superior sensitivity and stability of our experiment. For later analysis we calculate the V_G -dependent $\sigma_1(\omega)$ from the $T(V_G)/T(0)$ data [27–29] and show it in Figure 3(d).

With the nature of Peak-A been identified, the next question to be addressed is the origin of the initial state. Before we discuss this issue, we give further thoughts on the gate-dependent growth of Peak-A. Figure 3 implies that the SS-population will become stronger if E_F could be brought down further. The latter would be possible when V_G is applied to high value beyond the limit of our measurement, where such high-gating was in fact demonstrated experimentally [30]. Here we will consider how large Peak-A will grow in the strong-gating regime. In Figure 4a, we show the bulk interband transition in the mid-IR range. The onset energy ($\equiv E_{op}$) of this transition corresponds to the thick arrow in Fig.4(b). The E_{op} increases when the Fermi level shifts up. Fig.4(c) shows that the increase rate is $dE_{op}/dV_G = 1.74 \times 10^{-4} [\text{eV/V}] \equiv a$. In the mean time the $S = \int \sigma_1^A(\omega) d\omega$ calculated from Figure 3(d) decreases at the rate $ds/dV_G = -6.06 \times 10^{-4} [1/V] \equiv b$, where $s = S/S(0V)$ is the normalized S by ungated $S(0)$. Given a and b we can eliminate V_G and obtain the S -change against E_F as $ds/dE_F = (ds/dV_G) \cdot (dV_G/dE_F) = b/(a/2) = 6.96 [1/\text{eV}]$. Here $dV_G/dE_F = (a/2)^{-1}$ was derived by utilizing the Bernstein-Moss relation[31–33], namely, $dE_F/dV_G = \frac{1}{2} \times dE_{op}/dV_G = \frac{a}{2}$ where the factor $\frac{1}{2}$ comes from $\frac{1}{m_{CV}^*} = \frac{1}{m_{CB}^*} + \frac{1}{m_{VB}^*}$ and $m_{CB}^* = m_{VB}^*$ [34]. This result $ds/dE_F = 6.96 [1/\text{eV}]$ enables us estimate

S at high gating: For the pristine, electron-doped Bi_2Se_3 films like ours, the Fermi level lies typically at $E_F \sim 0.1\text{eV}$ from the CB bottom (CBB). If the gating shifts E_F down to the CBB, i.e, $\Delta E_F = 0.1$, then s will increase approximately by $\Delta s \approx [\frac{ds}{dE_F}] \cdot \Delta E_F = 0.69$. that is, Peak-A grows by $\sim 70\%$ compared with the ungated strength. If E_F is shifted further to the Dirac point, the latter lying $\sim 0.2\text{eV}$ from the CBB, we have $s = s(0) + \Delta s \approx 1 + [\frac{ds}{dE_F}] \cdot (0.1 + 0.2) = 3.09$. That is, Peak-A grows as large as three-times. (Here we assumed $\frac{ds}{dE_F}$ is constant for simplicity, neglecting its E_F -dependence.) This estimation shows that substantial increase of the peak will occur at high-gating. From this exercise we also learn that if S is precisely characterized as function of E_F , it could be used to determine the location of the Fermi level in Bi_2Se_3 films, whereas usually more difficult ARPES should be performed.

Discussion. We now search for possible candidate for the initial state of the Peak-A. For this we refer to the band structure of Bi_2Se_3 reported in experimental [3, 7, 35–39] and theoretical [40–43] literatures, and schematically redrew it in Figure 5. In Figure 5 note that there is an energy branch lying $\sim 1\text{eV}$ below the SS. Interestingly, this branch $E(k)$ runs in near-parallel with the SS. If we consider the optical transition from this $E(k)$ branch ($=i$) to SS ($=f$), their parallel dispersion $\nabla_k E^i(k) \cong \nabla_k E^f(k)$ leads to strong absorption due to that transition strength $S \sim \int \frac{M_{fi}}{|\nabla_k E^f(k) - \nabla_k E^i(k)|} d^2k$ becomes divergent. This yields a pronounced absorption at $\hbar\omega = E_f - E_i = 1\text{eV}$, which agrees with the profile of Peak-A. (Here the transition matrix element M_{fi} is assumed to be constant for simplicity.) Therefore this $1\text{eV}-E(k)$ is a plausible candidate for the i -state. We think that this assignment can be confirmed when theoretical calculation of $\sigma_1(\omega)$, not available currently, is performed. We remark that optical transition of Bi_2Se_3 between bulk and surface in particular was poorly studied so far with a rare exception[17]. To consider another candidate native defect such as Se-vacancy can produce defect levels below E_F . However their energy locations are not well known, and generally such localized, dispersionless levels do not fulfill the $\nabla_k E^i(k) \cong \nabla_k E^f(k)$ condition. We emphasize that, while supporting works should follow to definitely identify the 1eV -bulk $E(k)$ as origin of i -state, the occurrence of the optical population of SS in Bi_2Se_3 is evident judging from the properties of Peak-A we have unveiled regardless of the i -state origin.

To make further remark on the $T(V_G)/T(0)$ data, Fig.3(b) shows that gate-dependent change occurs in the Far-IR and mid-IR ranges also. Similar change was reported for bulk-insulating $(\text{Bi}_{1-x}\text{Sb}_x)_2\text{Te}_3$ films[44]. While for $(\text{Bi}_{1-x}\text{Sb}_x)_2\text{Te}_3$ the mid-IR modulation peaks at $\sim 0.3\text{eV}$, the modulation for Bi_2Se_3 occurs at higher energy, peaked at 0.45eV . This difference is attributed to that the interband transition taking place at $E_{op} = E_g + 2E_F$ is higher for Bi_2Se_3 where E_F is significant ($\sim 0.1\text{eV}$) compared with the insulating $(\text{Bi}_{1-x}\text{Sb}_x)_2\text{Te}_3$ where E_F is considered to be much lower. Also, while the modulations in mid-IR and far-IR inevitably contain contribution from both bulk and surface states, the modulation strength of the 1eV feature is weaker, which may further support the surface-related origin. Further quantitative analysis and comparison will be published separately.

In conclusion we performed broadband optical absorption measurement on pristine Bi_2Se_3 and In-substituted $(\text{Bi}_{1-x}\text{In}_x)_2\text{Se}_3$ thin films, as well as electrically gated Bi_2Se_3 . The absorption Peak-A that occurs at $\hbar\omega = 1\text{eV}$ showed clear correlation with the In-driven TI-NTI phase transition: it is activated at $x < x_c$ (TI-phase) but is completely vanished for $x > x_c$ (NTI) along with the quenching of the topological surface state. Furthermore, the Peak-A become stronger/weaker by the electron depletion/injection into the Bi_2Se_3 in the electrical gating measurement. The two experimental results provide convincing evidence that Peak-A arises from the population of SS, i.e, the optical excitation of electron from 1eV below into into SS. This SS-optical population increases the density of the surface electron, thus can enhance the topological electrical conduction, which promotes TI device application. Similar optically driven SS-population may be realized in other TI materials as well, which should be investigated in the future. *Note added:* For our $(\text{Bi}_{1-x}\text{In}_x)_2\text{Se}_3$ films, the bulk transition E_{op} shows a different x -dependent behavior from Ref.[25]. It may come from that carrier doping due to Se-vacancy is sample-dependent for these TI films. See Supplemental Fig.S3[20].

Acknowledgments. This work was supported by the 2016 sabbatical year research grant of the University of Seoul. JM and SO are supported by the Gordon and Betty Moore Foundations EPiQS Initiative (GBMF4418) and National Science Foundation (NSF) grant EFMA-1542798.

-
- [1] L. Fu, C. L. Kane, and E. J. Mele, Physical Review Letters **98**, 106803 (2007).
 [2] Y. Xia, D. Qian, D. Hsieh, L. Wray, A. Pal, H. Lin, A. Bansil, D. Grauer, Y. S. Hor, R. J. Cava, *et al.*, Nature Physics **5**, 398 (2009).
 [3] M. Z. Hasan and C. L. Kane, Reviews of Modern Physics

- 82**, 3045 (2010).
 [4] J. E. Moore, Nature **464**, 194 (2010).
 [5] X.-L. Qi and S.-C. Zhang, Reviews of Modern Physics **83**, 1057 (2011).
 [6] P. Roushan, J. Seo, C. V. Parker, Y. S. Hor, D. Hsieh, D. Qian, A. Richardella, M. Z. Hasan, R. J. Cava, and

- A. Yazdani, *Nature* **460**, 1106 (2009).
- [7] D. Hsieh, Y. Xia, D. Qian, L. Wray, J. Dil, F. Meier, J. Osterwalder, L. Patthey, J. Checkelsky, N. Ong, *et al.*, *Nature* **460**, 1101 (2009).
- [8] C. Li, O. Vant Erve, J. Robinson, Y. Liu, L. Li, and B. Jonker, *Nature Nanotechnology* **9**, 218 (2014).
- [9] R. V. Aguilar, A. Stier, W. Liu, L. Bilbro, D. George, N. Bansal, L. Wu, J. Cerne, A. Markelz, S. Oh, *et al.*, *Physical Review Letters* **108**, 087403 (2012).
- [10] K. Post, B. Chapler, M. Liu, J. Wu, H. Stinson, M. Goldflam, A. Richardella, J. Lee, A. Reijnders, K. Burch, *et al.*, *Physical Review Letters* **115**, 116804 (2015).
- [11] E. Falsetti, A. Nucara, P. P. Shibayev, M. Salehi, J. Moon, S. Oh, J.-B. Brubach, P. Roy, M. Ortolani, and P. Calvani, *Physical Review Letters* **121**, 176803 (2018).
- [12] P. Di Pietro, M. Ortolani, O. Lima, A. Di Gaspare, V. Giliberti, F. Giorgianni, M. Brahlek, N. Bansal, N. Koirala, S. Oh, *et al.*, *Nature Nanotechnology* **8**, 556 (2013).
- [13] C. In, S. Sim, B. Kim, H. Bae, H. Jung, W. Jang, M. Son, J. Moon, M. Salehi, S. Y. Seo, *et al.*, *Nano Letters* **18**, 734 (2018).
- [14] J. McIver, D. Hsieh, H. Steinberg, P. Jarillo-Herrero, and N. Gedik, *Nature Nanotechnology* **7**, 96 (2012).
- [15] Z. Yue, G. Xue, J. Liu, Y. Wang, and M. Gu, *Nature Communications* **8**, 15354 (2017).
- [16] J. A. Sobota, S.-L. Yang, A. F. Kemper, J. Lee, F. T. Schmitt, W. Li, R. G. Moore, J. G. Analytis, I. R. Fisher, P. S. Kirchmann, *et al.*, *Physical Review Letters* **111**, 136802 (2013).
- [17] L. Li, W. Xu, and F. Peeters, *Journal of Applied Physics* **117**, 175305 (2015).
- [18] N. Bansal, Y. S. Kim, E. Edrey, M. Brahlek, Y. Horibe, K. Iida, M. Tanimura, G.-H. Li, T. Feng, H.-D. Lee, *et al.*, *Thin Solid Films* **520**, 224 (2011).
- [19] A. Kuzmenko, *Review of Scientific Instruments* **76**, 083108 (2005).
- [20] See Supplemental Material at [URL will be inserted by the production group] for additional data of the Bi 2 Se 3.
- [21] K. Post, B. Chapler, L. He, X. Kou, K. L. Wang, and D. Basov, *Physical Review B* **88**, 075121 (2013).
- [22] P. Di Pietro, F. Vitucci, D. Nicoletti, L. Baldassarre, P. Calvani, R. Cava, Y. Hor, U. Schade, and S. Lupi, *Physical Review B* **86**, 045439 (2012).
- [23] M. Brahlek, N. Bansal, N. Koirala, S.-Y. Xu, M. Neupane, C. Liu, M. Z. Hasan, and S. Oh, *Physical Review Letters* **109**, 186403 (2012).
- [24] M. Salehi, H. Shapourian, N. Koirala, M. J. Brahlek, J. Moon, and S. Oh, *Nano Letters* **16**, 5528 (2016).
- [25] L. Wu, M. Brahlek, R. V. Aguilar, A. Stier, C. Morris, Y. Lubashevsky, L. Bilbro, N. Bansal, S. Oh, and N. Armitage, *Nature Physics* **9**, 410 (2013).
- [26] S. Sim, N. Koirala, M. Brahlek, J. H. Sung, J. Park, S. Cha, M.-H. Jo, S. Oh, and H. Choi, *Physical Review B* **91**, 235438 (2015).
- [27] K. Yu, J. Kim, J. Y. Kim, W. Lee, J. Y. Hwang, E. Hwang, and E. Choi, *Physical Review B* **94**, 235404 (2016).
- [28] K. Yu, J. Jeon, J. Kim, C. W. Oh, Y. Yoon, B. J. Kim, J. H. Cho, and E. Choi, *Applied Physics Letters* **114**, 083503 (2019).
- [29] K. Yu, B. V. Laun, T. S. Kim, J. Jeon, J. Kim, P. Moon, Y. H. Lee, and E. Choi, Submitted (2019).
- [30] N. Bansal, N. Koirala, M. Brahlek, M.-G. Han, Y. Zhu, Y. Cao, J. Waugh, D. S. Dessau, and S. Oh, *Applied Physics Letters* **104**, 241606 (2014).
- [31] E. Burstein, *Physical Review* **93**, 632 (1954).
- [32] T. Moss, *Proceedings of the Physical Society. Section B* **67**, 775 (1954).
- [33] I. Hamberg, C. G. Granqvist, K.-F. Berggren, B. E. Sernelius, and L. Engström, *Physical Review B* **30**, 3240 (1984).
- [34] J. G. Analytis, J.-H. Chu, Y. Chen, F. Corredor, R. D. McDonald, Z. Shen, and I. R. Fisher, *Physical Review B* **81**, 205407 (2010).
- [35] I. Nechaev, R. Hatch, M. Bianchi, D. Guan, C. Friedrich, I. Aguilera, J. Mi, B. Iversen, S. Blügel, P. Hofmann, and E. Chulkov, *Physical Review B* **87**, 121111 (2013).
- [36] Z.-H. Pan, E. Vescovo, A. Fedorov, D. Gardner, Y. Lee, S. Chu, G. Gu, and T. Valla, *Physical Review Letters* **106**, 257004 (2011).
- [37] L. A. Wray, S.-Y. Xu, Y. Xia, Y. San Hor, D. Qian, A. V. Fedorov, H. Lin, A. Bansil, R. J. Cava, and M. Z. Hasan, *Nature Physics* **6**, 855 (2010).
- [38] A. Dubroka, O. Caha, M. Hronček, P. Friš, M. Orlita, V. Holý, H. Steiner, G. Bauer, G. Springholz, and J. Humlíček, *Physical Review B* **96**, 235202 (2017).
- [39] B. A. Piot, W. Desrat, D. K. Maude, M. Orlita, M. Potemski, G. Martinez, and Y. S. Hor, *Physical Review B* **93**, 155206 (2016).
- [40] I. Aguilera, C. Friedrich, G. Bihlmayer, and S. Blügel, *Physical Review B* **88**, 045206 (2013).
- [41] M. Guo, Z. Wang, Y. Xu, H. Huang, Y. Zang, C. Liu, W. Duan, Z. Gan, S.-C. Zhang, K. He, *et al.*, *New Journal of Physics* **18**, 015008 (2016).
- [42] T. Förster, P. Krüger, and M. Rohlffing, *Physical Review B* **91**, 035313 (2015).
- [43] M. Hermanowicz and M. W. Radny, *Physica Status Solidi (RRL)–Rapid Research Letters* **13**, 1800460 (2019).
- [44] W. S. Whitney, V. W. Brar, Y. Ou, Y. Shao, A. R. Davoyan, D. N. Basov, K. He, Q.-K. Xue, and H. A. Atwater, *Nano letters* **17**, 255 (2016).

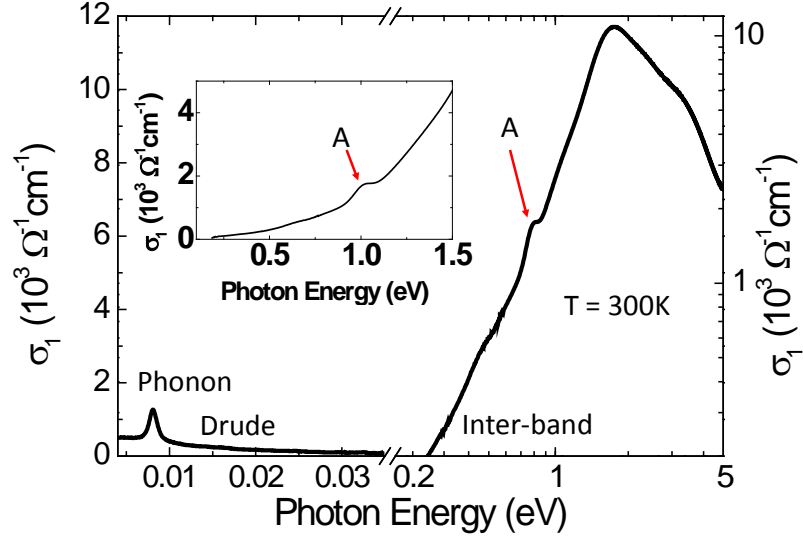


FIG. 1. **Optical conductivity of Bi_2Se_3 thin film ($d=50\text{QL}$)** $\sigma_1(\omega)$ shows the Drude, phonon, and interband transition. Note that log-log scale is used for the $0.2\text{eV} \leq \hbar\omega \leq 5\text{eV}$ range. Inset shows the Peak-A in the real scale.

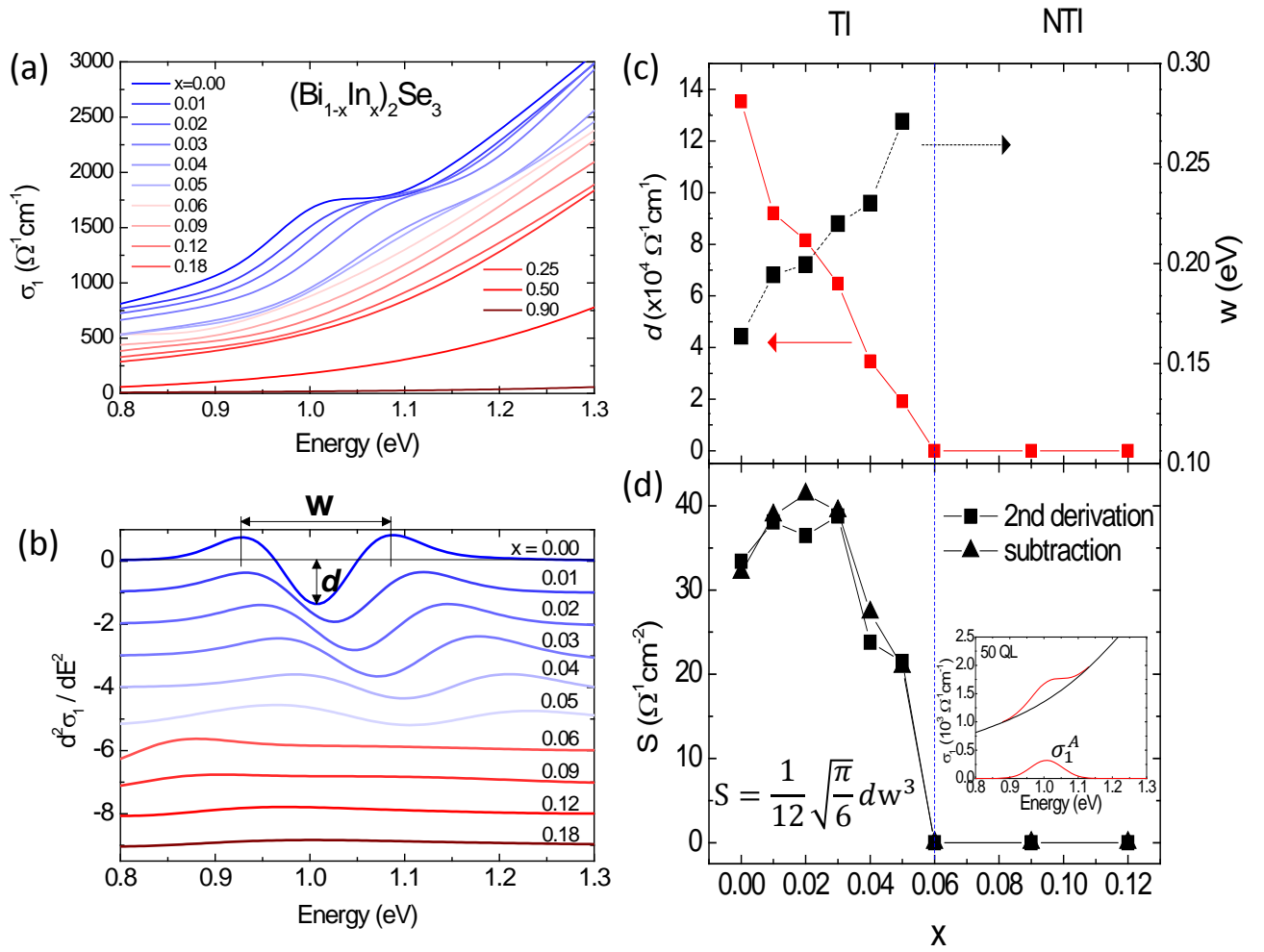


FIG. 2. **Evolution of Peak-A in In-substituted $(\text{Bi}_{1-x}\text{In}_x)_2\text{Se}_3$ thin films.** (a) optical conductivity of $(\text{Bi}_{1-x}\text{In}_x)_2\text{Se}_3$ for the In-concentration range of $0 \leq x \leq 0.9$. (b) The second derivate of optical conductivity $\frac{d^2\sigma_1}{dE^2}$. The x -dependent behavior of Peak-A can be traced more clearly in this plot. Here w and d denote the distance between the two maxima and depth of the dip, respectively. (c) The width w and depth d are shown as function of x . (d) The peak strength S calculated from $S = \frac{1}{12} \sqrt{\frac{\pi}{6}} dw^3$ (see Supplemental Fig.S1[20]). We also calculate S by $S = \int \sigma_1^A(\omega) d\omega$ where $\sigma_1^A(\omega) = \sigma_1(\omega) - \sigma_1^{BG}(\omega)$ (σ_1^{BG} = polynomial background) as shown in the inset. In (c) and (d), the critical concentration $x_c=0.06$ of the TI to non-TI (NTI) phase transition is highlighted by the vertical line.

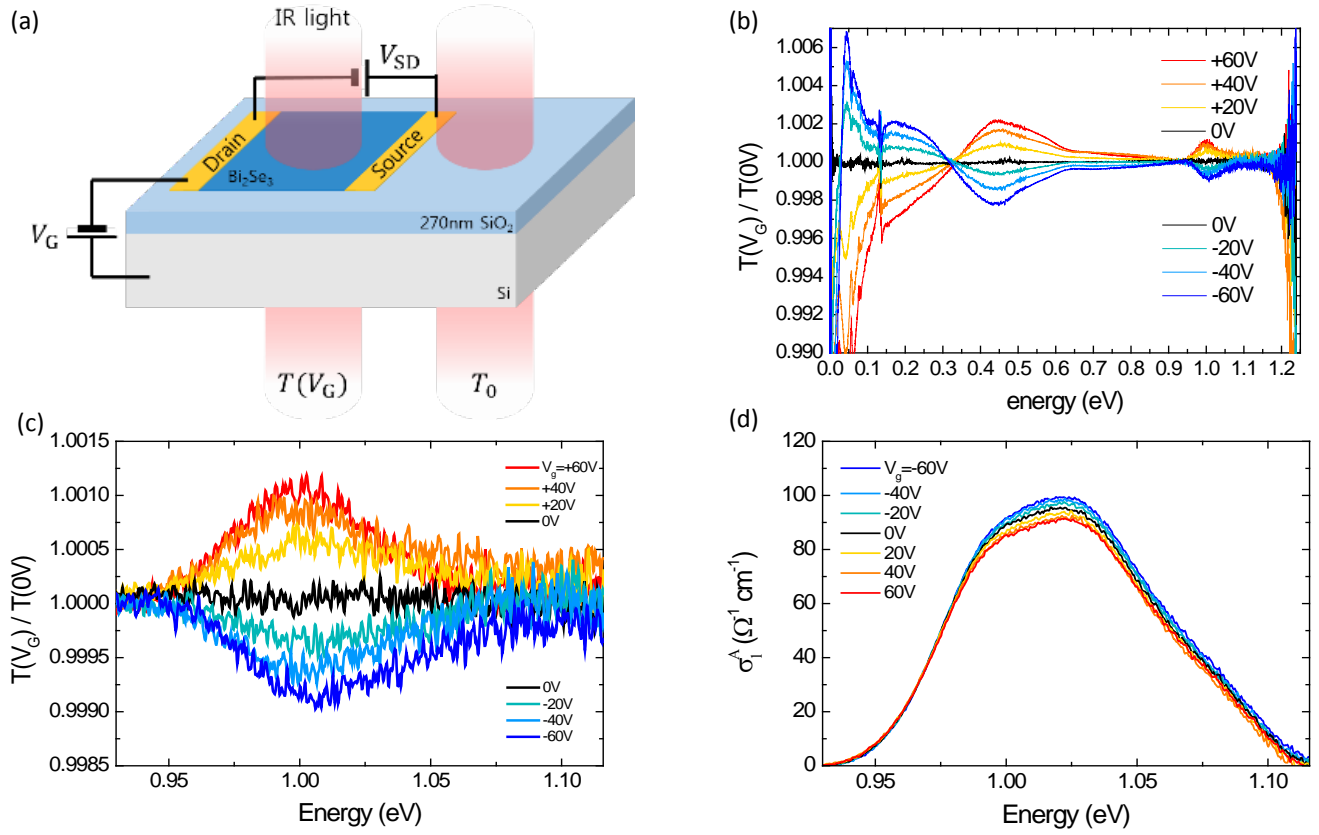


FIG. 3. **Gate-driven change of Bi_2Se_3 .** (a) Schematic diagram of gate-controlled transmission measurement of Bi_2Se_3 thin film. $T(V_G)$ is taken with the bias voltage V_G applied between the film and Si. (b) $T(V_G)/T(0)$ changes in the Far-IR, mid-IR, and at 1eV. (c) For peak-A $T(V_G)$ increases/decreases for the negative/positive V_G , respectively. (d) Optical conductivity of Peak-A, $\sigma_1^A(\omega)$, was calculated from $T(V_G)$ in (c) as described in the text.

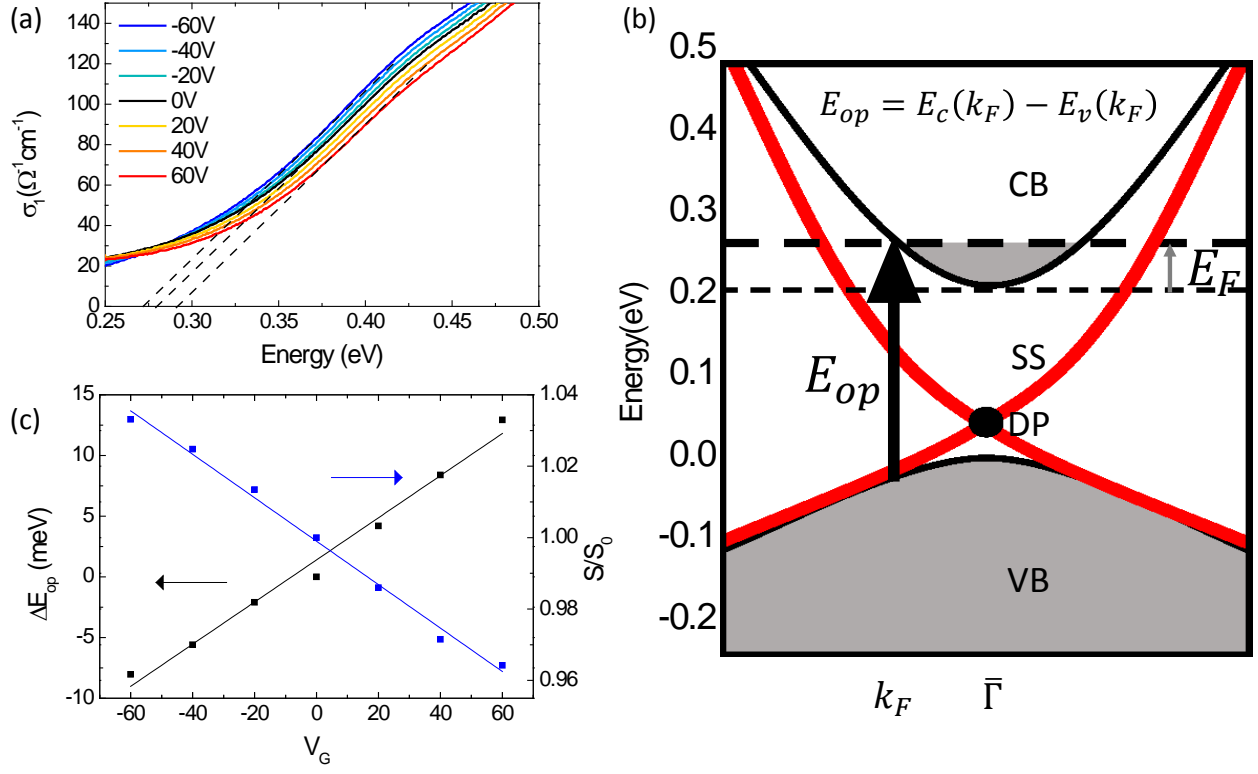


FIG. 4. **Estimation of the growth of Peak-A at high gating voltage.** (a) Gate-driven shift of the inter-band transition. The onset energy E_{op} is determined by the linear extrapolation of data (dashed line). (b) Schematic diagram of the VB \rightarrow CB interband transition. The E_{op} corresponds to onset of the VB \rightarrow CB. Here the Fermi energy E_F is measured from the CB bottom. DP stands for Dirac point. (c) The shift $\Delta E_{op} = E_{op}(V_G) - E_{op}(0)$ and the change of S are plotted against V_G . Here S was calculated by integrating $\sigma_1(\omega)$ in Figure 3c as $S = \int \sigma_1^A(\omega) d\omega$.

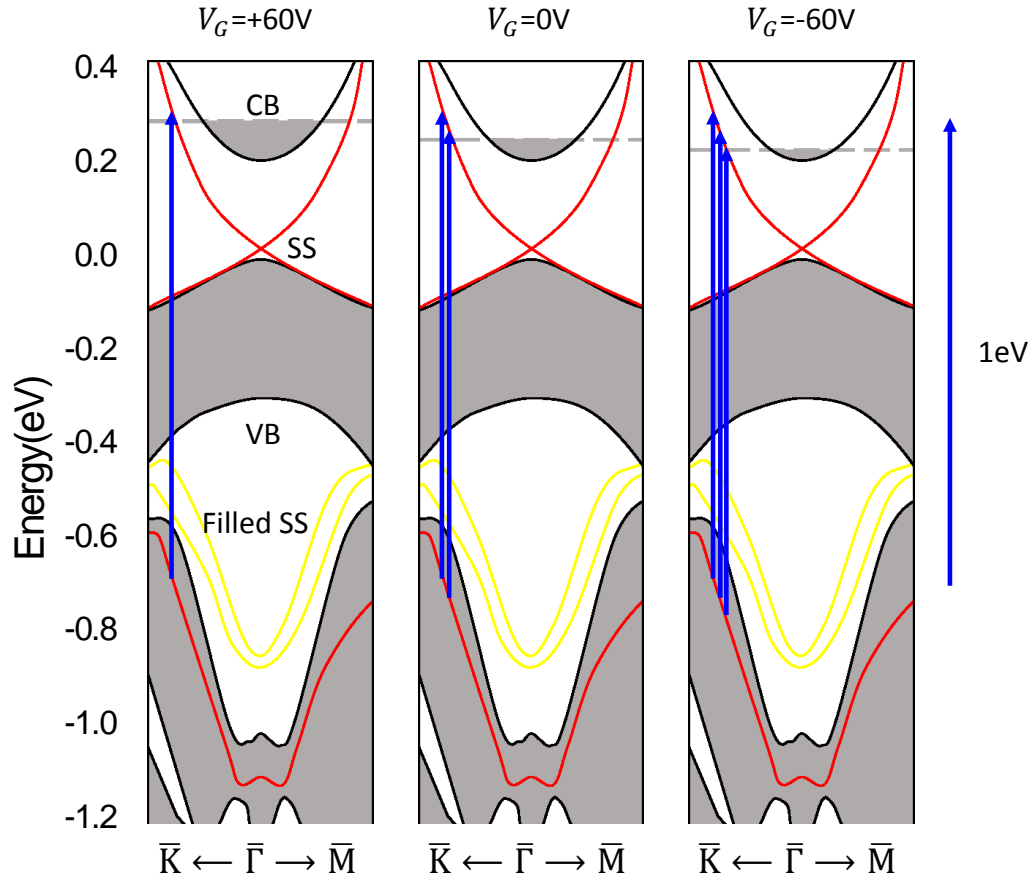


FIG. 5. **Schematic band structure and possible origin of Peak-A.** For $V_G=0$, electron is excited from the bulk band branch into the empty surface state as highlighted by the blue arrows. For the positive gating, the Fermi level E_F shifts up and the 1eV- transition becomes weaker. For the negative gating E_F shifts down and the 1eV- transition becomes stronger. The amount of E_F -shift is exaggerated for clarity. The band diagram shown here was redrawn schematically based on experiment [3, 7, 35–39] and theory [40–43]. CB=bulk conduction band, VB=bulk valence band, SS=surface state.